Article:

Zhang, C., Maramizonouz, S., Yang, C. et al. (3 more authors) (2025) Electro-mechanical insights into the mixing of conductive and non-conductive sands at an interface. Powder Technology, 458. 120991. ISSN 0032-5910

https://doi.org/10.1016/j.powtec.2025.120991

Powder Technology 458 (2025) 120991

Contents lists available at ScienceDirect

Powder Technology

journal homepage: www.journals.elsevier.com/powder-technology

Electro-mechanical insights into the mixing of conductive and non-conductive sands at an interface

Chao Zhang [a], Sadaf Maramizonouz [a], Changrong Yang [a], David Milledge [a], Roger Lewis [b], Sadegh Nadimi [a,*]

[a] School of Engineering, Newcastle University, Newcastle upon Tyne NE1 7RU, United Kingdom
[b] Department of Mechanical Engineering, The University of Sheffield, Sheffield S1 3JD, United Kingdom

HIGHLIGHTS

- Mixing conductive and non-conductive sands enhances interfacial electrical isolation.
- Small fraction of conductive sand significantly reduces the interface resistance.
- A heatmap is produced to estimate the percentage of conductive sand required.
- Heatmap links the resistivity of various sands with their required percentage.

GRAPHICAL ABSTRACT

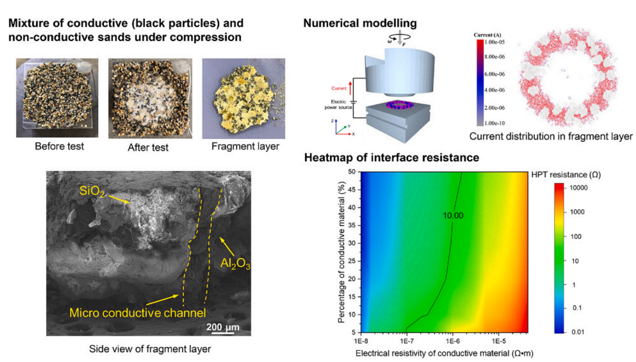

ARTICLE INFO

Keywords:
Discrete element method
Electro-mechanical coupling
Particles
Sands

ABSTRACT

This paper investigates the electrical behaviour of an electrically conductive sand particle when mixed with non-conductive silica sand, commonly used in the railway industry. Laboratory tests and numerical simulations are conducted to assess the effect of mixing on the electrical conduction properties at the metal-to-metal interface under mechanical loading. Results from compression tests demonstrate that mixing with even 5 % mass of conductive particles can significantly reduce electrical resistance at the interface; however, the decrease in electrical resistance gradually slows down when the mixing ratio of conductive particles exceeds 10 %. Discrete element modelling of high pressure torsion tests – enhanced with a newly proposed electro-mechanical contact model – reveal that fine conductive particles are more effective than coarse particles in reducing interfacial electrical resistance at equal mixing ratios. A heatmap is proposed to estimate the percentage of conductive particles required to bring the resistance of the interface below the critical threshold of 10 Ω for track circuit, which links the resistivity of various conductive particles with their required mixing ratio.

* Corresponding author.
E-mail address: sadegh.nadimi-shahraki@newcastle.ac.uk (S. Nadimi).

https://doi.org/10.1016/j.powtec.2025.120991
Received 15 January 2025; Received in revised form 27 March 2025; Accepted 27 March 2025
Available online 28 March 2025

1. Introduction

A key component in railway operations is the use of detection systems to locate trains [1]. In the UK, railway tracks are divided into blocks, each forming a "track circuit" designed to detect trains. These track circuits, typically bounded by insulated joints, operate by transmitting an electrical signal from a transmitter at one end of the section to a detector at the other end [1]. When a train occupies a block, the track circuit is shorted out, thereby allowing the system to detect the presence of the train. However, when contaminants (e.g., leaf layers) accumulate at the wheel-rail interface, this can result in electrical isolation, potentially preventing the system from detecting the train [2]. The Rail Safety and Standards Board (RSSB) [3] in Great Britain has indicated that contaminants are responsible for 97 % of all instances of electrical isolation between wheels and rails.

Since the early days of the railway industry, sanding has been employed as a solution to mitigate low adhesion[1] conditions at the wheel-rail interface [4]. This method is crucial in situations where the adhesion between the wheel and rail is insufficient to ensure effective braking and acceleration of the train. In addition, surface roughness of sand particles [5] and inter-particle friction [6], can influence the mechanical behaviour of the particulate systems at both macro- and microscopic scales. These effects, then, can impact the transmission of electrical current within the particulate system [7], potentially disrupting the proper operation of track circuits [8]. According to research by the RSSB [3], only 3 % of instances of electrical isolation between wheel and rail are attributable to sand application. This conclusion is based on current sand usage rates, which are restricted to 7.5 g/m. If more sand is applied to further minimise the effects of low adhesion due to more difficult conditions (e.g., oil [9], water [10], oxides [11]), there will be an increased risk of rail isolation.

There have been several studies investigating the electrical isolation at the wheel-rail interface [12,13] and trying to offer solutions on how to alleviate its adverse effects [7,14,15]. To examine the impact of sand particles on electrical isolation, twin-disc tests were conducted [12,13] which showed that larger sand particles and lower sand flowrates decrease electrical isolation. However, the geometrical scale and the operational conditions of the twin-disc set-up are vastly different from real-world applications and thus should only be considered as "a guide to what will happen in the full-size wheel-rail contact" [12,13]. Chapteuil et al. [14] used Discrete Element Method (DEM) to numerically model the presence of a copper/graphite mixture at the wheel-rail interface. Though highly simplified and qualitative by design, their results demonstrated that an optimal copper/graphite ratio could achieve a balance between electrical and tribological properties. Skipper et al. [7,16] utilised a high pressure torsion (HPT) test set-up to explore changes in electrical resistance and adhesion at the wheel-rail interface, using several newly developed conductive particles as alternatives to standard rail-sand. Their findings showed that Product B and D particles significantly reduced resistance even in leaf-contaminated conditions, and also effectively mitigated low adhesion. Zhang et al. [15] numerically simulated the same HPT set-up utilising their novel electro-mechanical contact model implemented into DEM to study the electro-mechanical behaviour of two types of electrically conductive particles as well as the standard rail-sand. The combined findings of Skipper et al. [7] and Zhang et al. [15] indicate that substituting conductive particles for the standard rail-sand can enhance electrical conduction at the interface but the associated costs of manufacturing these commercial conductive particles could pose a significant constraint.

In addition, several studies have investigated particle breakage [17], entrainment efficiency [18], and traction effects at the wheel-rail interface [19] using experiments and numerical simulations, offering some guidance for understanding the relationship between traction improvement and track circuit compatibility. Suhr et al. [17] developed a DEM model to simulate sand particle breakage under dry and wet conditions, successfully capturing fragment diffusion and solidified cluster formation. Maramizonouz et al. [18] used CFD-DEM coupling to model sanding at wheel-rail interface, showing that particle density, size, shape, and uniformity significantly impact entrainment efficiency, with flat and elongated particles achieving 50 % and 30 % higher entrainment rates than spherical ones. Skipper et al. [19] studied wheel-rail contact under low adhesion conditions using an HPT test, finding that harder and less round particles improve traction, especially in leaf-contaminated environments. However, these studies do not yet provide a practical solution for balancing adhesion performance and electrical isolation in railway applications.

To reduce costs, the usage of commercial conductive particles could be reduced by mixing them with standard rail-sand. The effects of mixing conductive and non-conductive particles on the electrical conduction of the wheel-rail interface and determining the optimal mixing ratios to specifically regulate the electrical behaviour remain an open scientific challenge. This study aims to investigate the electro-mechanical properties of mixed conductive and non-conductive sand particles at the wheel-rail interface. A 1-D compression test and HPT modelling are utilised to examine the fragmentation behaviour and contact mechanics of mixed particles under load, as well as to investigate the effects of these mixtures and their mixing ratios on electrical response at the interface. To evaluate the contribution of conductive and non-conductive particle mixtures to electrical conduction under adverse conditions, a worst-case scenario of wheel-rail contact—specifically, the electrical response of a light vehicle, which induces a contact pressure of 600 MPa at wheel-rail interface when passing through sand fragment layer—is conducted [7,20]. If the particle mixture enhances electrical conductivity in such challenging conditions, it is likely to be effective in less severe scenarios as well. The findings contribute to ongoing efforts to enhance railway safety and performance by providing a cost-effective approach to managing electrical isolation challenges.

2. Experimental investigation

2.1. Testing set-up

Fig. 1a shows a modified one-dimensional (1-D) compression test for measuring the electrical resistance at metal-to-metal interface. The piston and the base specimens are both fabricated from O1 tool steel, which is hardened and tempered to 58–60 Rockwell C grade hardness, with high resistance to abrasion and toughness to ensure the test can be completed under high pressure conditions. The piston specimen is a cylinder with a diameter of 35 mm and a height of 50 mm. The dimensions of the base specimen are 50 mm × 50 mm × 40 mm. In addition, a circuit is developed to measure the electrical resistance between the piston and the base specimens when they are in contact, as shown in Fig. 1b. To prepare the circuit mentioned above, the piston and base specimens are sanded using 400-grit silicon carbide abrasive paper to ensure that the surfaces are smooth. Then, an electronic glue is used to adhere the wires to the surfaces of the specimens and keep good electrical contact between them, and the wires are fixed by using hot-melt adhesive. A TENMA 72-7732A Digital Multimeter is used, which applies a constant current and then measures the electrical resistance value between the interface of the piston and the base specimen using the instrument's voltmeter.

The test materials are spread evenly on the base specimen and then the piston specimen is placed on the top of the materials. The spherical platen is positioned directly above the piston specimen to ensure parallel alignment, preventing uneven loading in the system. Moreover, an electrically insulating lubricating layer is applied to the surface of the spherical platen, as shown in Fig. 1c. This arrangement ensures that

[1] In the railway industry "adhesion" or "adhesion coefficient" is defined as the amount of traction present when the wheel-rail contact enters partial slip. In this paper, the terms are used interchangeably.

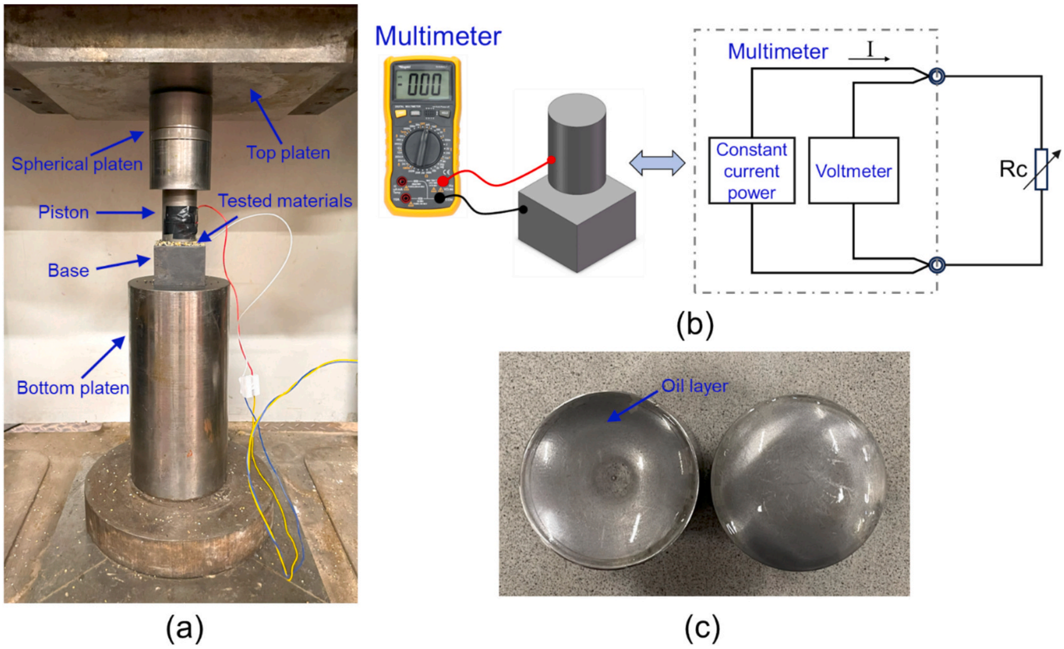

Fig. 1. (a) 1-D compression test set-up for measuring electrical resistance at the interface between piston and base specimens, (b) schematic of a simple circuit used in the compression test, and (c) spherical platen with electrically insulated lubrication coating.

current flows only through the closed circuit between the piston and the base specimens.

2.2. Particle characteristics

The results of particle characterisation by Maramizonouz et al. [21] and HPT testing by Skipper et al. [7] indicated that the sand-like commercial conductive particles (referred to as Product D for confidentiality) are a type of alumina particles with a coating and are particularly promising for further investigation. Therefore, silica sand and Product D particles are selected for compression tests, the latter having an electrical resistivity ranging from 1.66×10^{-8} Ω·m to 4.31×10^{-5} Ω·m [21]. These two types of particles are shown in Fig. 2a and b, respectively. The particle size distribution (PSD) of silica sand and Product D are characterised through sieve analysis following BS1377–2:1990 [22], and their PSD is presented in Fig. 2c. It can be seen that PSD of these two materials ranges from 0.6 mm to 2 mm. More details on the other particle characteristics of these two materials can be found in the previous work [21].

Powder X-ray Diffraction (XRD) of product D and silica sand particles is performed by a Bruker D2 Phaser with LynxEye detector using Cu Kα radiation. For phase identification of finely ground samples, the diffraction parameters including divergence slit, 2θ range, step size and step-1 are set to 1.0 mm, 10–100°, 0.033° and 0.5 s, respectively. The phase compositions of Product D and silica sand particles are shown in Fig. 3. The highest diffraction peak of Product D particles, located at 2θ = 53°, is identified as the Al_2O_3 phase (reference code 96–100-0033) [21]. For silica sand particles, the principal peak appears at 2θ = 27°,

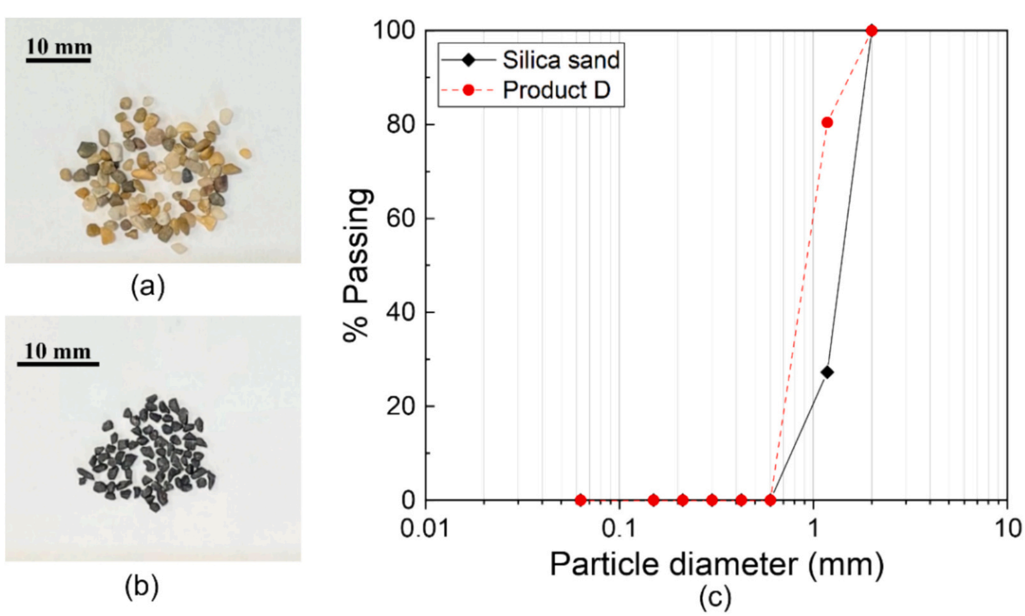

Fig. 2. (a) Photos of silica sand and (b) Product D used in the tests, (c) particle size distribution of the two tested materials obtained by sieve analysis.

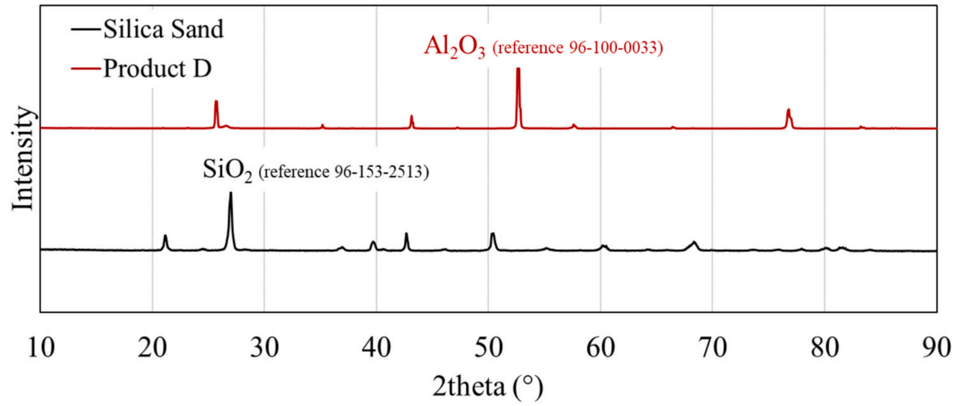

Fig. 3. XRD spectrum of the Product D and silica sand particles.

corresponding to the SiO_2 (quartz) phase (reference code 96–153-2513) [21]. To ensure the reliability of these XRD results, they are corroborated with Scanning Electron Microscope (SEM) and Energy-Dispersive X-ray (EDX) analyses provided by the School of Engineering at Newcastle University, United Kingdom.

2.3. 1-D compression test scenarios

To investigate the effect of silica sand and Product D particles, both individually and in combination, on the interfacial electrical resistance between the piston and the base specimens, the experimental scenarios employed in this study are listed in Table 1. Following the practice of Skipper et al. [7], a total mass of 10 g particles is used in each test. This quantity ensures complete physical separation between the piston and the base specimen throughout the experiment, preventing direct metal-to-metal contact and allowing the particles to fully occupy the interface. The test scenarios in Table 1 are systematically designed to examine the influence of different mixing ratios on electrical resistance. Two extreme cases are first defined: one consisting entirely of Product D particles and the other consisting solely of sand particles. Afterwards, the mass of Product D particles is gradually increased from 0.5 g while maintaining a total mixture of 10 g, allowing for a controlled investigation of how electrical resistance transitions across different mixing ratios. To ensure the reliability of the results, each test scenario is repeated three times.

Table 1
Mass of Product D and silica sand particles in each test scenario.

Test No.	Silica sand (g)	Product D (g)
1	10	0
2	9.5	0.5
3	9	1
4	8	2
5	7	3
6	5	5
7	0	10

For sample preparation before each test, a precision balance (±0.001 g) is utilised to weight silica sand and Product D particles following Table 1, with a total sample mass of 10 g. A standard sieve stack collection pan with a sieve lid is used to mix the two particle types by manually shaking for around 15 s. A cylindrical steel ring with inner diameter of 35 mm, 7 mm wall thickness, and height of 40 mm is positioned at the centre of base specimen to minimise particle loss and ensure uniform placement. The mixed particles are air-pluviated into the ring using a funnel, after which the ring is carefully removed. The piston specimen is then gently placed on top of the deposited mixture, and the compression test is carried out. During each test, a loading force is applied at a rate of 20 kN while continuously recording the electrical resistance across the interface. Once the loading force reaches 577 kN, corresponding to a contact pressure of 600 MPa between the piston and

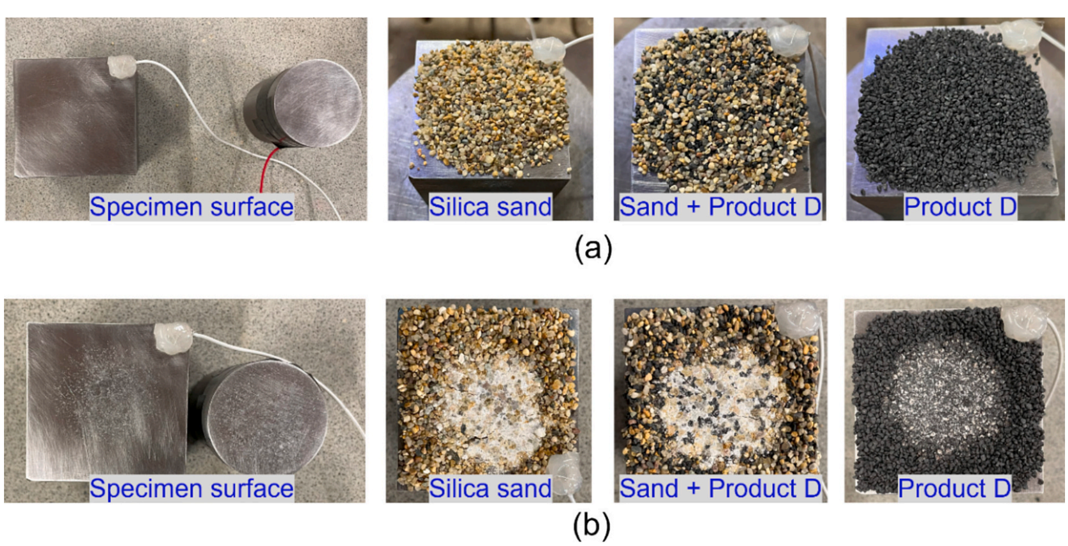

Fig. 4. Photos of the surfaces of the piston and the base specimens, accompanied by silica sand particles (10 g), a mixture of silica sand (5 g) and Product D particles (5 g), and Product D particles (10 g): (a) before test, (b) after test.

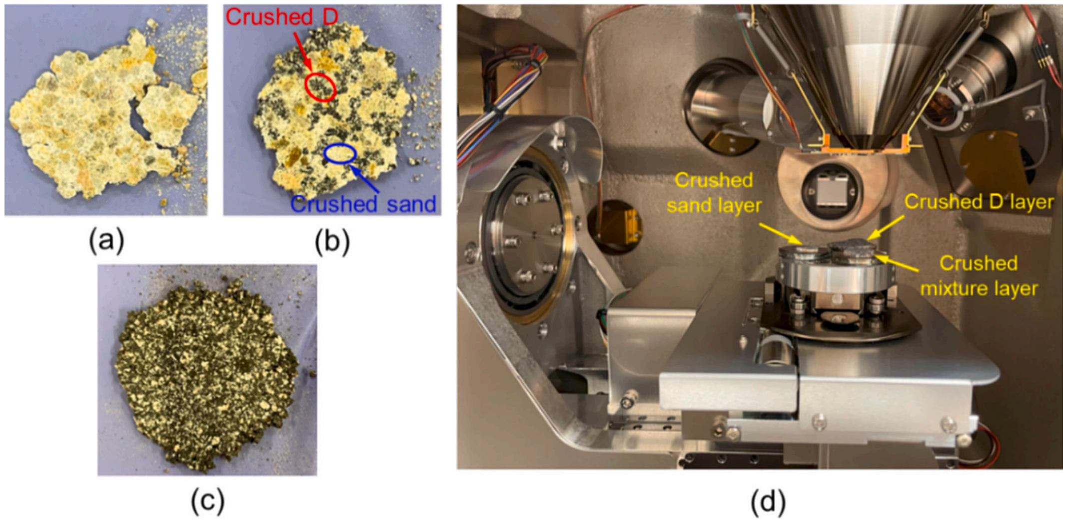

Fig. 5. Photos of fragment layer of crushed (a) silica sand (10 g), (b) mixture of silica sand (5 g) and Product D (5 g), (c) Product D particles (10 g) and (d) SEM analysis.

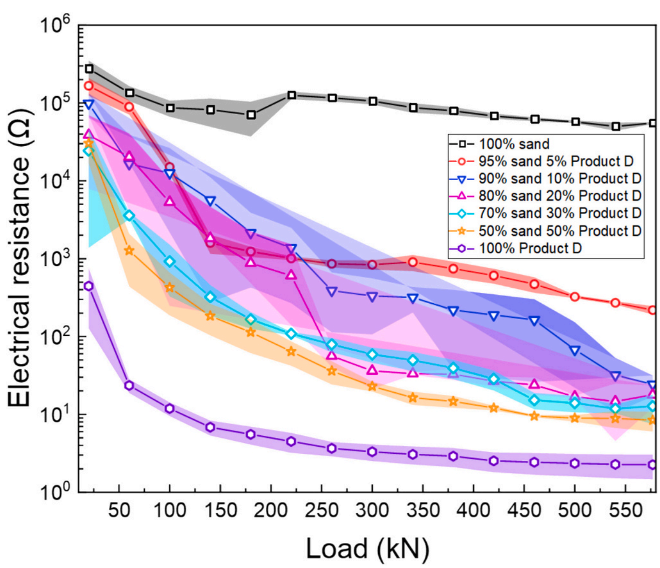

Fig. 6. Variation of electrical resistance at the interface between piston and base specimen with increasing mechanical loads for different mixing ratios of Product D and silica sand.

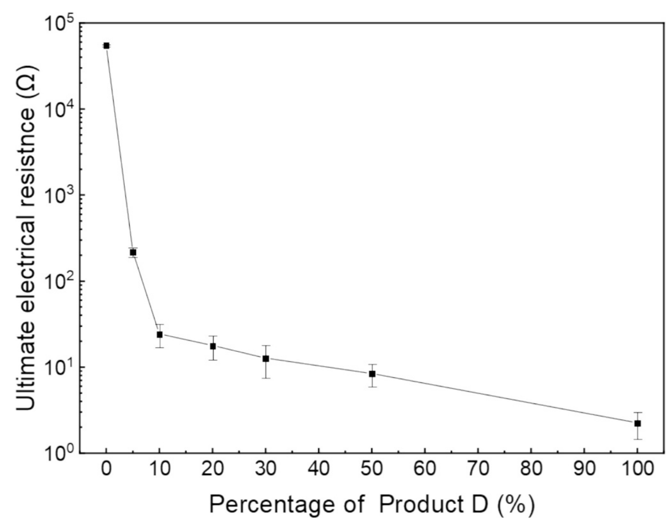

Fig. 7. Ultimate electrical resistance at the interface between piston and base specimen versus the percentage of Product D particles under constant normal mechanical load (ultimate electrical resistance is the measured resistance value after 10 s of constant 600 MPa contact pressure).

the base specimen [20], it is maintained for 10 s, and the stabilised electrical resistance values are measured and recorded.

Silicon carbide abrasive paper is used to polish both the piston and base specimens before each test to ensure a smooth surface finish. Fig. 4a and b display examples of the surfaces of the piston and the base specimens before and after each test, including silica sand particles (Test No.1), a mixture of silica sand and Product D particles (Test No.6), and Product D particles (Test No.7).

2.4. Scanning electron microscopy

After completing each 1-D compression test, the fragment layer formed at the interface between the piston and the base specimen due to particle fragmentation is collected. The fragment layers obtained from silica sand particles (Test No.1), a mixture of silica sand and Product D particles (Test No.6), and Product D particles (Test No.7) are shown in Fig. 5a, b and c, respectively. To analyse the microstructure of the different fragment layers, Scanning Electron Microscopy (SEM) technique (JSM-IT510, JEOL Ltd., Japan) is utilised as presented in Fig. 5d.

2.5. Effect of conductive particle content on interfacial electrical resistance

Fig. 6 shows the evolution of the electrical resistance at the interface between the piston and the base specimens under mechanical loading for various mixing ratios of Product D and silica sand particles. The figure clearly shows the electrical isolation between the interface of the piston and the base specimens when the test material is 100 % sand particles. However, for each mixing scenario, a significant decrease in the interfacial electrical resistance is shown as mechanical loading increases. Previous studies suggest that as the mechanical loading increases, the contact area between two metal particles expands and the oxide layer on the surface of the particles is crushed, leading to the formation of more conductive micro-channels in the oxide film, through which current can be transferred [23,24]. This means that the fragment

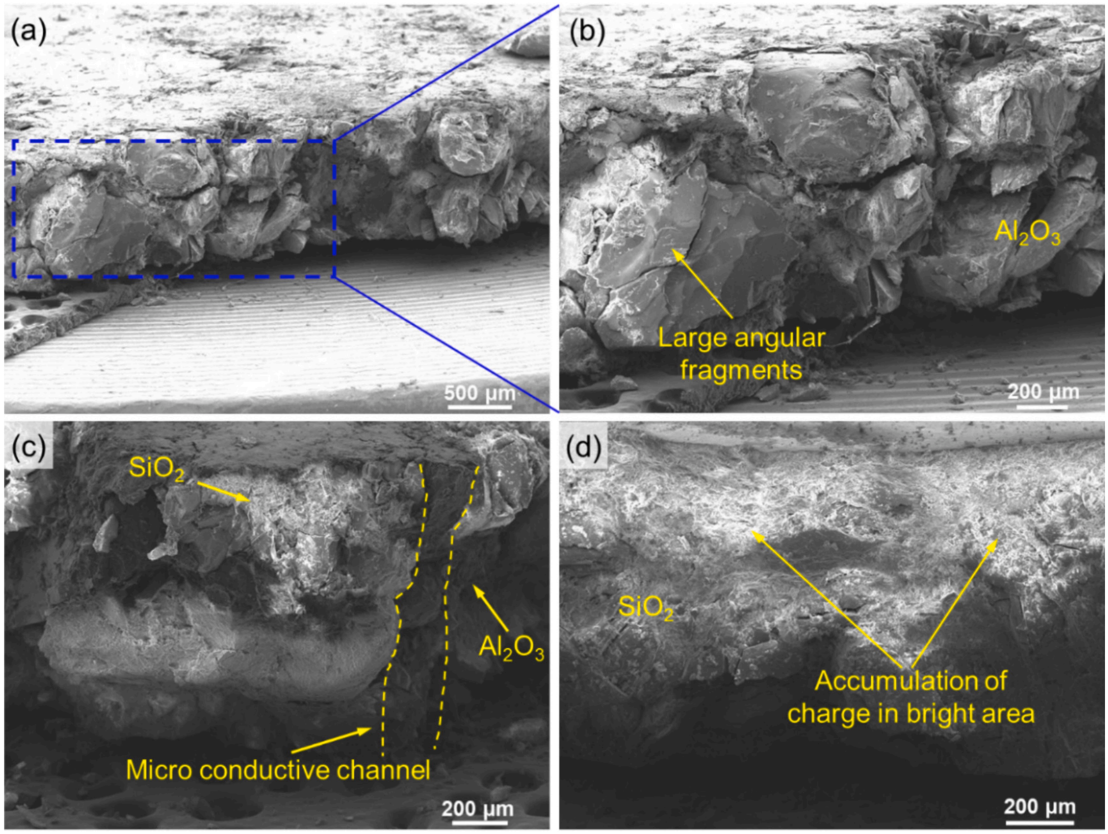

Fig. 8. SEM images of the side of the fragment layer: (a) Product D particles (10 g) (b) zoomed in view of Product D particles, (c) mixture of Product D (5 g) and silica sand particles (5 g), and (d) silica sand particles (10 g).

layer has a similar mechanism to the oxide film, and the current can be transferred along the conductive micro-channels. For 100 % silica sand particles, a higher load increases the contact area between the fragments and the specimen surfaces after sand fragmentation; however, the intrinsic electrical properties of the sand impede current transmission within the fragment layer. Instead, when Product D particles are included, their contact area with the piston and the base specimens increases under high contact pressure, leading to more conductive micro-channels within the fragment layer.

Fig. 7 displays the correlation between mixing ratios (Product D: silica sand particles) and the interfacial electrical resistance when the load reaches 577 kN, i.e. a contact pressure of 600 MPa at the interface between the piston and base specimens. A significant drop in the ultimate electrical resistance at the metal-to-metal interface is observed when the mixing ratio increases. In particular, the interfacial electrical resistance falls abruptly from ~55 kΩ to ~220 Ω when the percentage of conductive particles is raised from 0 % to 5 %. This sharp decline indicates that Product D particles effectively enhance the conduction performance of the fragment layer and establish good electrical contacts with the specimens. In addition, the ultimate electrical resistance at the interface between piston and base specimen becomes progressively smaller as the percentage of Product D particles increases. However, the decrease in the ultimate electrical resistance is most pronounced as the percentage of Product D increases from 0 % to 10 %, and particularly from 0 % to 5 %.

2.6. Fragment layer microstructure

The SEM images depicted in Fig. 8 reveal the morphological characteristics and layered structure of different composite particles. The thickness of each fragment layer is around 1 mm and can become densely packed after Product D particles (Test No.7) are crushed under high contact pressure (Fig. 8a and b). Mechanical loading causes some particles to break, and the resulting fragments are compacted and interlocked, forming a relatively homogeneous texture with larger angular fragments. Additionally, the uniform brightness of the fragment layer observed in the SEM images, combined with the XRD results from Fig. 3, suggests that the fragments are primarily composed of Al_2O_3 crystals. These crystals effectively dissipate electrons, helping to prevent the accumulation of charges. Fig. 8c shows the fragment layer generated by crushing a mixture of Product D and silica sand particles (Test No.6), with the interface between the two particles clearly visible. The distinct contrast between the bright and dark areas in the image suggests that SiO_2 may be concentrated in the bright regions. This concentration could promote localised charging, potentially leading to an accumulation of charge in these areas. It is also notable that Al_2O_3 crystals are interspersed in the matrix, showing that mechanical interlocking may exist between these particles and that conductive micro-channels are established in the fragment layer. The fragment layer of silica sand particles (Test No.1) exhibits a relatively uniform texture and composition (Fig. 8d). The high brightness in Fig. 8d suggests that SiO_2 is evenly distributed throughout the matrix, leading to charge accumulation. This charge build-up underscores the difficulty in forming conductive micro-channels in the fragmented silica sand layer, suggesting that the material properties of silica sand impede the efficient transfer of current through the fragments.

3. Numerical investigation

A numerical model of the HPT test is set up to investigate changes in electrical resistance when a mixture of conductive and non-conductive particles is applied to the wheel-rail interface under relatively high contact pressure conditions.

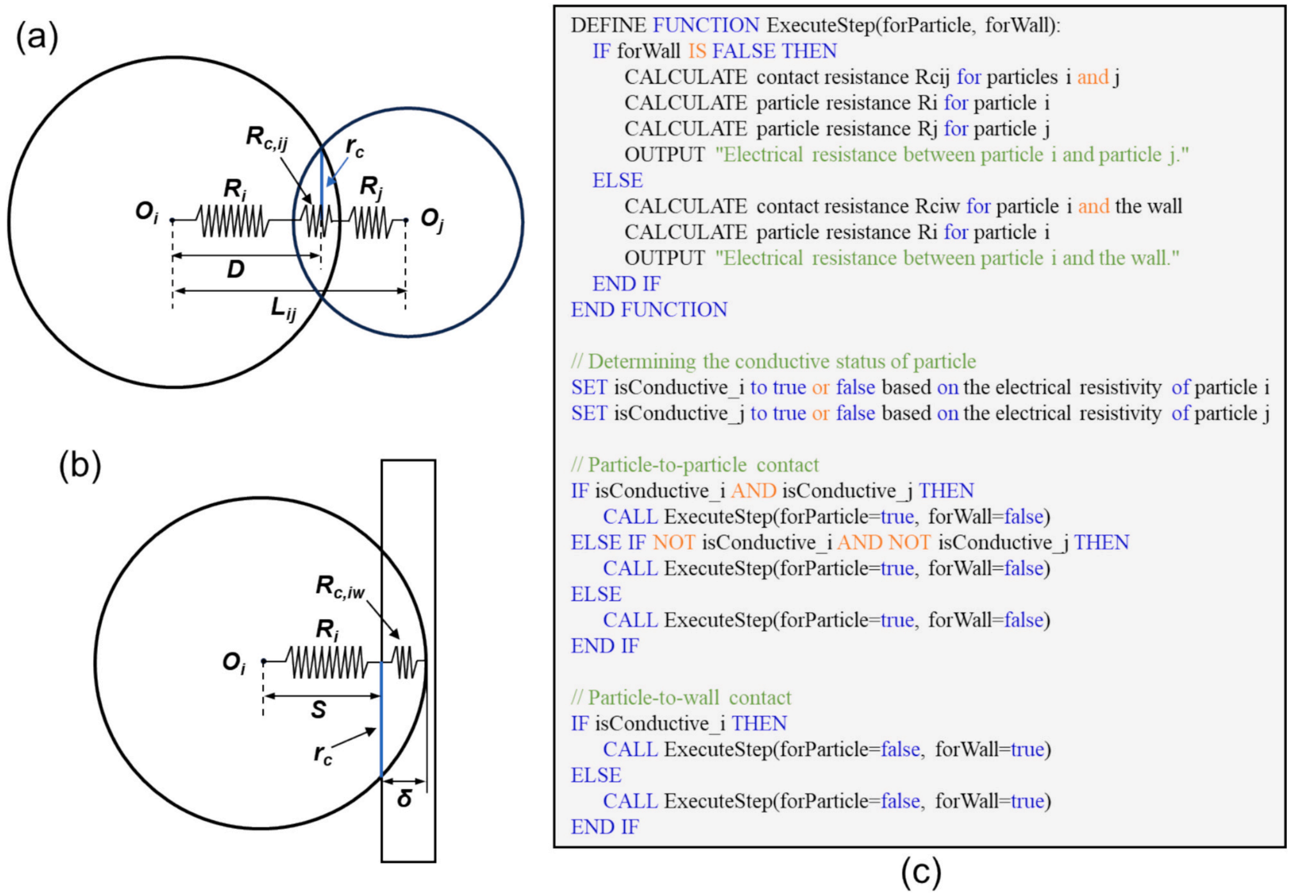

Fig. 9. Schematic of the components of the resistance when two objects are in contact, including their geometric characteristics, together with a pseudo-code for calculating the corresponding resistance: (a) particle-to-particle contact, (b) particle-to-wall contact, (c) pseudo-code.

3.1. Electro-mechanical contact model

For a particulate system connected to a direct current (DC) circuit, an electro-mechanical contact model in authors' previously published work [15] is employed to evaluate its electrical properties. The motion of the particles is modelled using DEM, with Newton's second law and Euler's law used to describe the translational and rotational motion of individual particles [25,26]:

$$m_i\frac{d\overrightarrow{v}_i}{dt} = \sum_{j=1,j\neq i}\left(\overrightarrow{F}^n_{c,ij} + \overrightarrow{F}^t_{c,ij}\right) + m_i\overrightarrow{g} \tag{1}$$

$$I_i\frac{d\overrightarrow{\omega}_i}{dt} = \sum_{j=1,j\neq i}\left(r_i \times \overrightarrow{F}^t_{c,ij} + \overrightarrow{M}_{r,i}\right) \tag{2}$$

where $\overrightarrow{v_i}$, ω_i, m_i, I_i, r_i and $M_{r,i}$ are defined as translational velocity, angular velocity, mass, moment of inertia, particle radius, and the rolling resistance torque of particle *i*. $F^n_{c,ij}$ and $F^t_{c,ij}$ are contact forces in the normal and tangential directions, respectively, when particle *j* acts on particle *i*. Additionally, *g* is the gravitational acceleration.

As the particles are moving under load, contacts occur between particles or between particles and the wall. During this process, electrons flow freely from one conductive object to another through the contact region, constructing a conductive path [27]. A reasonable analogy can be drawn between contact paths in a particulate system and an electrical circuit, following the nodal analysis method [28,29]. For two particles in contact, each particle is regarded as a node and the path between the particle centres as a branch. Fig. 9a illustrates the electrical resistance (R_{ij}) on the conductive path of particle-to-particle contact:

$$R_{ij} = R_i + R_{c,ij} + R_j \tag{3}$$

where R_i, $R_{c,ij}$, and R_j are defined as the particle resistance from the centre of particle *i* to the contact plane, the contact resistance between two contacting particles, and the particle resistance from the contact plane to the centre of particle *j*.

In this regard, the contact resistance can be solved using the Holm resistance model [30], while the particle resistance can be calculated based on the geometric transformation characteristics between the two particles in contact. Therefore, Eq. (3) can be written in the following form:

$$R_{ij} = \int_0^{r_i-\delta_i} \rho_i\frac{dz}{\pi\left(r_i^2 - z^2\right)} + \frac{\rho_i + \rho_j}{4r_c} + \int_0^{r_j-\delta_j} \rho_j\frac{dz}{\pi\left(r_j^2 - z^2\right)} \tag{4}$$

where ρ_i and r_i are defined as the electrical resistivity and radius of particle *i*, while ρ_j and r_j are the electrical resistivity and radius of particle *j*. δ_i and δ_i are the overlaps arising from contact between the particle *i* and particle *j*, respectively. r_c is the contact radius for two contacting particles, which can be solved by the classical Hertz theory [26,31]. In addition, *D* and L_{ij} are the distances from the centre of particle *i* to the contact plane and between the centres of the two overlapping particles, respectively. These distances can be determined via the characteristics of the geometrical transitions of particles in contact. Therefore, Eq. (4) can be written as follows:

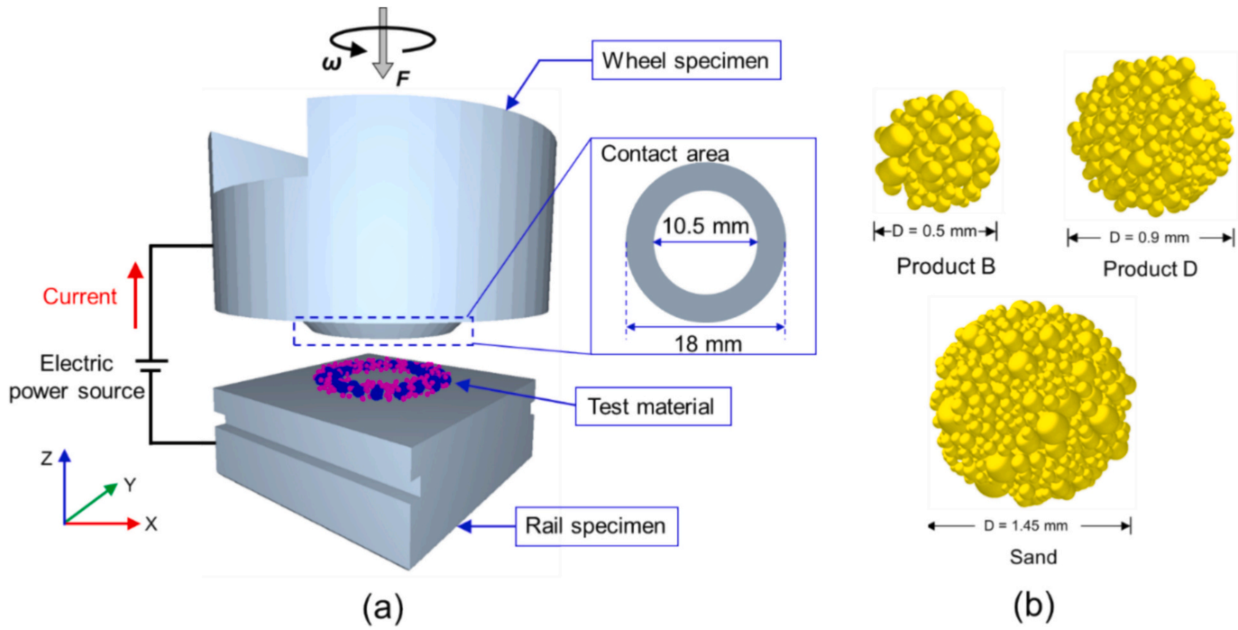

Fig. 10. (a) The simulation set-up for HPT tests connected to a DC circuit, where the normal load is applied before torsion begins and (b) modelling of cluster particles for silica sand, Product B and Product D with a diameter of d50 (the pink particles represent Product B while the blue particles represent sand). (For interpretation of the references to colour in this figure legend, the reader is referred to the web version of this article.)

$$R_{ij} = \frac{\rho_i}{2\pi r_i}\ln\left(\frac{r_i^2 - r_j^2 + L_{ij}^2 + 2r_iL_{ij}}{r_j^2 - r_i^2 - L_{ij}^2 + 2r_iL_{ij}}\right) + \frac{1}{2}(\rho_i + \rho_j)\sqrt[3]{\frac{E^*}{6f_nr^*}} + \frac{\rho_j}{2\pi r_j}\ln\left(\frac{r_j^2 - r_i^2 + L_{ij}^2 + 2r_jL_{ij}}{r_i^2 - r_j^2 - L_{ij}^2 + 2r_jL_{ij}}\right) \tag{5}$$

where E^*, f_n, and r^* are defined as the equivalent Young's modulus, the normal contact force, and the effective radius, respectively.

To calculate the resistance R_{iw} for particle-to-wall contact, as shown in Fig. 9b, the contact resistance $R_{c,iw}$ between the particle i and the wall should be considered, as well as the particle resistance R_i from the centre of particle i to the contact plane of the wall:

$$R_{iw} = R_i + R_{c,iw} \tag{6}$$

The contact resistance between the particle and the wall follows the same method as for the particle-to-particle contact, while the distance from the centre of the particle to the contact plane is S. Then, Eq. (6) can be written as:

$$R_{iw} = \int_0^S \rho_i \frac{dz}{\pi(r_i^2 - z^2)} + \frac{\rho_i + \rho_w}{4r_c'} \tag{7}$$

where ρ_w and r_c' are the electrical resistivity of the wall and contact radius when the particle is in contact with the wall. The overlap δ between a particle i and the wall due to loading is used to determine the distance S. Therefore, Eq. (7) can be written as follows:

$$R_{iw} = \frac{\rho_i}{2\pi r_i}\ln\left(\frac{2r_i}{\delta} - 1\right) + \frac{1}{2}(\rho_i + \rho_w)\sqrt[3]{\frac{E^*}{6f_nr_i}} \tag{8}$$

After determining the electrical resistance of the particle-to-particle and particle-to-wall contacts, and then incorporating Ohm's law and Kirchhoff's current law allows the electrical properties of the entire particulate system to be estimated. The electromechanical contact model is then implemented in the EDEM™ software package [32] using the C++ programming language. Moreover, in a particulate system consisting of conductive and non-conductive particles, a classification of the type with respect to particle-to-particle and particle-to-wall contacts under loading is required. For particle-to-particle contacts, three categories are identified: (i) two conductive particles, (ii) one conductive and one non-conductive particle, and (iii) two non-conductive particles. Particle-to-wall contacts are classified into: (i) conductive particle-wall contact and (ii) non-conductive particle-wall contact. The particle's electrical resistivity is used to determine whether it is conductive or not, and the appropriate contact classification is applied based on this property. Fig. 9c shows the pseudo-code of the complete computational workflow for calculating the resistance of particle-to-particle and particle-to-wall contacts.

3.2. *High pressure torsion tests*

This section analyses the effects of mixing Product D or a finer conductive material (Product B, with median diameter d50 = 0.5 mm [15]) with silica sand particles on the electrical conduction properties at the wheel-rail interface in the HPT system. Numerical simulations are used to investigate how these mixtures, and the use of conductive particles of different sizes, influence interface conductivity. An example of the HPT simulation set-up with a mixture of Product B and silica sand particles at the contact area of the wheel and rail specimens is shown in Fig. 10a. A constant voltage of 0.5 V is imposed to the wheel specimen, while the rail specimen is maintained at 0 V, effectively simulating a DC circuit, with 0.5 V_{DC} representing the worst-performing low-voltage DC track circuit in the UK railway operations [33]. A normal load is applied to the wheel specimen to achieve a contact pressure of 600 MPa at the wheel-rail interface to simulate a light vehicle with an axle load of approximately 80 kN [20]. This is because a light vehicle is less capable of breaking down the contamination layer, leading to weak conductive performance at the wheel-rail interface. For dynamic similarity, dimensionless analysis is used to scale down the contact pressure from 600 MPa to 6 MPa [34]. During the above process, the whole HPT system constitutes a closed circuit, and the current is transmitted from the wheel specimen to the rail specimen via the fragment layers. When the wheel specimen does not continue to displace and the contact pressure at the wheel-rail interface reaches 6 MPa, a uniform angular velocity of 1 deg./s is applied to the rail specimen. Meanwhile, the collected voltage and current data can be used to calculate the electrical resistance of the

Table 2
Simulation parameters utilised in the HPT test.

Simulation parameters	Value		
Particle properties	Product B	Product D	Silica sand
Poisson's ratio (–)	0.3	0.3	0.3
Density (kg/m^3)	3.81×10^4	3.75×10^4	2.65×10^4
Young's modulus (Pa)	7×10^8	7×10^8	7×10^8
Particle diameter (mm)	0.5	0.9	1.45
Fragment diameter (mm)	0.06–0.2	0.06–0.3	0.06–0.38
Electrical resistivity (Ω·m)	1×10^{-6}	1×10^{-6}	5.56×10^6
Geometry properties	Wheel specimen	Rail specimen	
Poisson's ratio (–)	0.28	0.3	
Density (kg/m^3)	7850	7850	
Young's modulus (E)	2.3×10^{11}	2.1×10^{11}	
Electrical resistivity (Ω·m)	1.43×10^{-7}	1.43×10^{-7}	
Bond properties			
Normal stiffness (N/m^3)		1×10^{10}	
Shear stiffness (N/m^3)		1×10^{10}	
Critical normal stress (Pa)		1×10^8	
Critical shear stress (Pa)		1×10^8	
Interaction properties			
Coefficient of restitution (–)		0.8	
Coefficient of static friction (–)		0.5	
Coefficient of rolling friction (–)		0.01	

HPT system.

To model the conductive and non-conductive particles, d50 in the PSD curve obtained by sieving is selected as the diameter of particles. Laser diffraction is used to analyse the size distribution of fragments from crushed conductive and non-conductive particles collected from the railhead. From this data, spherical elements representing the corresponding fragment sizes are generated using an in-house Python code. In addition, the bonded particle model (BPM) [35] is used to reproduce the fragmentation behaviour of conductive and non-conductive particles under the mechanical loading. Each cluster particle is composed of individual spherical elements that are bonded together with finite-sized bonds. Detailed information on the breakage process of the particles at the wheel-rail interface can be found in the authors' previously published work [36]. The models of cluster particles for Product B, Product D and silica sand used in the HPT simulation are shown in Fig. 10b. The simulation parameters for the HPT test are listed in Table 2, which are taken from [7,15,16,36].

3.3. Mixing scenarios

To locate the mixed particles at the interface between the wheel and rail specimens, a geometry bin in the shape of a cylindrical shell with the same inner and outer diameters as the wheel-rail contact area (Fig. 10a) and a height of 2 mm is created. Following the operations of the previously published HPT simulation [15], a consistent volume fraction of the mixture is maintained to ensure that there is no direct contact between the wheel and rail specimens. The simulated mixing scenarios for Product B with silica sand and Product D with silica sand are shown in

Table 3
Mixing scenarios of conductive and non-conductive particles in the HPT simulation.

Case No.	Conductive particle			Non-conductive particle		
	Product B			Silica sand		
	Number of particles	Volume ratio (%)	Mass ratio (%)	Number of particles	Volume ratio (%)	Mass ratio (%)
a1	52	5	7	41	95	93
a2	105	10	13.7	39	90	86.3
a3	210	20	26.7	34	80	73.3
a4	315	30	38.2	30	70	61.8
a5	524	50	58.4	22	50	41.6
	Product D			Silica sand		
	Number of particles	Volume ratio (%)	Mass ratio (%)	Number of particles	Volume ratio (%)	Mass ratio (%)
b1	9	5	6.9	41	95	93.1
b2	17	10	12.9	39	90	87.1
b3	38	20	27.4	34	80	72.6
b4	55	30	38.3	30	70	61.7
b5	88	50	57.5	22	50	42.5

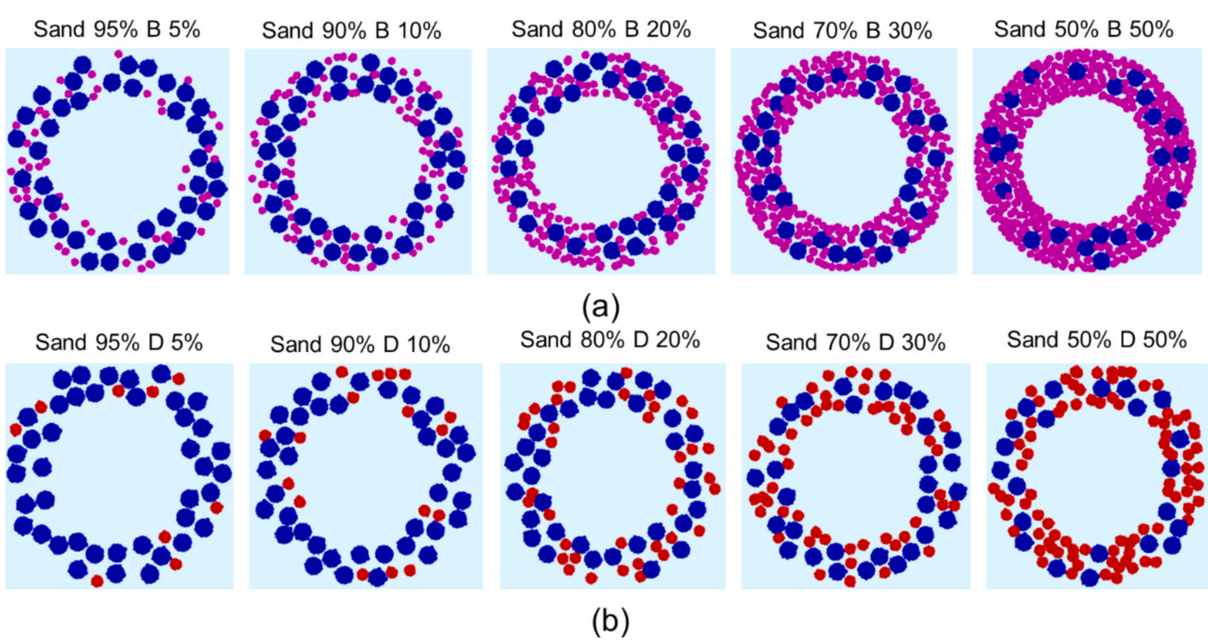

Fig. 11. Simulation scenarios with various mixing ratios of conductive and non-conductive particles: (a) mixing of silica sand and Product B, (b) mixing of silica sand and Product D (The blue, pink, and red clump particles represent silica sand, Product B, and Product D, respectively). (For interpretation of the references to colour in this figure legend, the reader is referred to the web version of this article.)

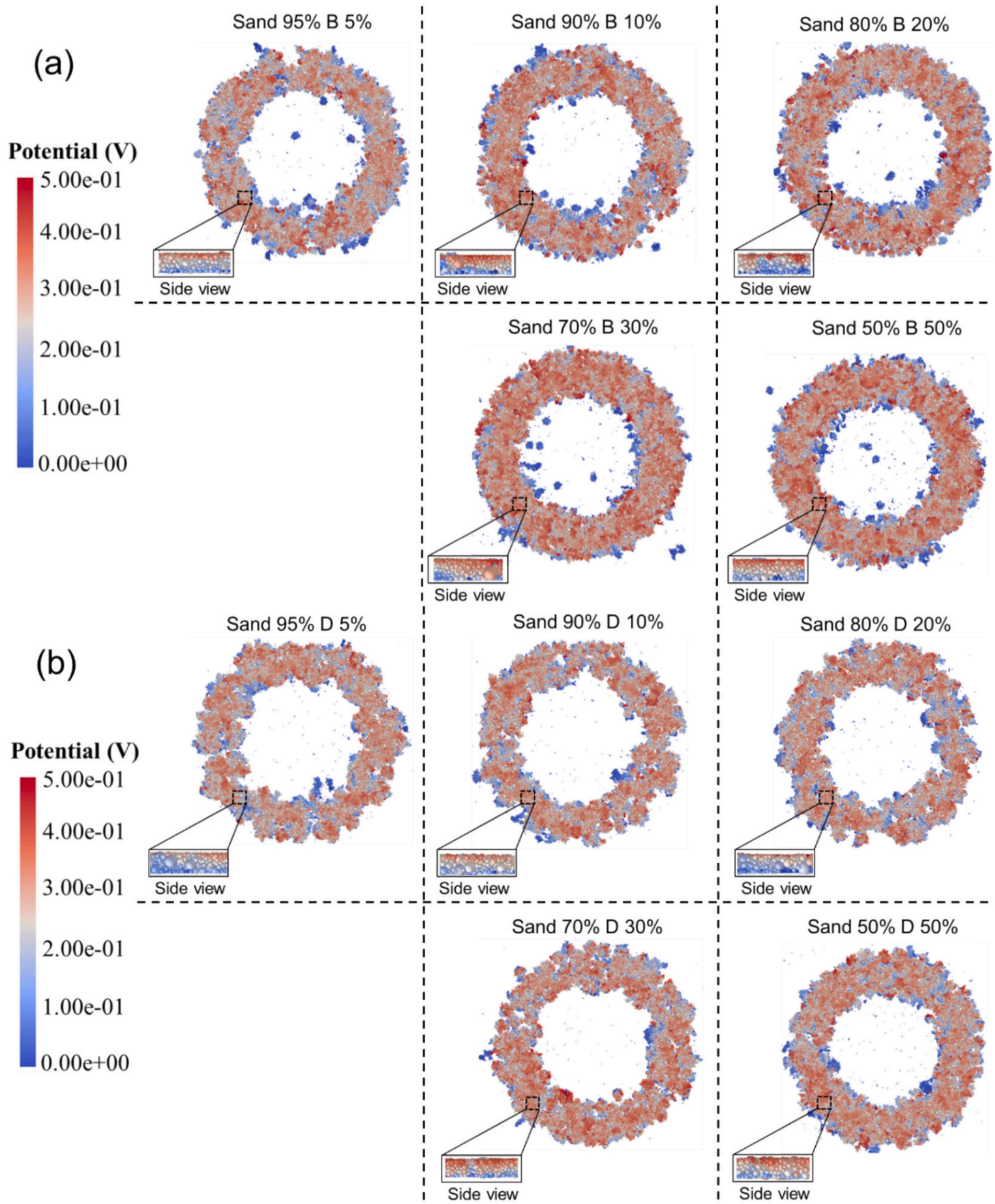

Fig. 12. Snapshots of the electric potential distribution in the fragment layer at the end of simulation for silica sand mixed with (a) Product B and (b) Product D, and (c) compare the number of fragments at the upper surface of the fragment layer greater than 0.3 V in each scenario for Products B and D.

Fig. 11a and b, respectively. In addition, the number of particles, the volume ratio, and the mass ratio of conductive and non-conductive particles under each simulation scenario are listed in Table 3.

3.4. Simulation results

Fig. 12a and b show the electric potential distribution of the fragment layer in the wheel-rail contact region for silica sand particles mixed with Product B and Product D, respectively. As the number of conductive particles increase, the interlocking between the crushed conductive fragments and sand fragments induced by mechanical loading makes the fragmented layer denser. In addition, fragments from conductive particles are interspersed in the matrix, and thus the potential distribution on the upper surface of the fragment layer gradually becomes more even as the percentage of conductive particles increases. Fig. 12c visually supports this statement, showing that as the percentage of conductive particles increases, the number of fragments with a potential exceeding 0.3 V on the upper surface rises apparently, particularly for Product B particles.

Fig. 13 presents the current intensity distribution in the fragment layer after a mixture of conductive and non-conductive particles is crushed in each mixing scenario. As shown in Fig. 13a, increasing the percentage of Product B particles leads to a noticeable rise in current intensity across most areas of the fragment layer. Mixing the crushed Product B fragments in the fragment layer results in the creation of conductive micro-channels which facilitate current transfer, similar to Fig. 8c. Also, as the fragment layer becomes denser and more uniform, the interaction between the fragments becomes stronger, leading to improved transmission of the electric current across the fragments (from side view). The trend of the current intensity distribution in the

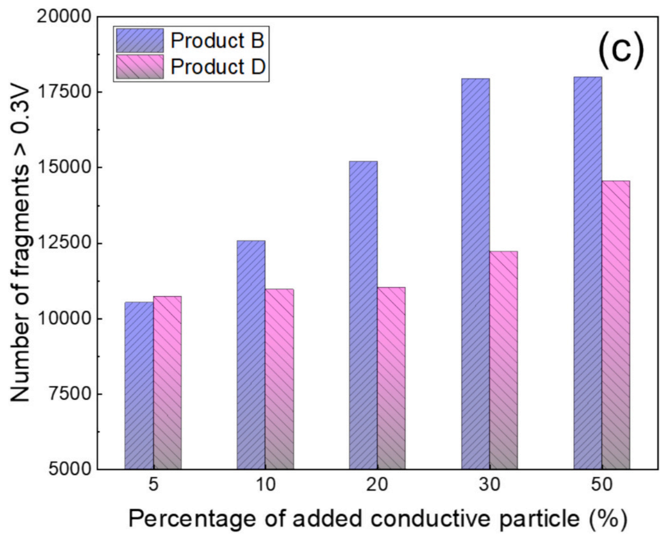

Fig. 12. (*continued*).

fragment layer for a mixture of Product D and silica sand particles is shown in Fig. 13b, which is generally consistent with Fig. 13a.

Fig. 14a and b show the variation of electrical resistance for the HPT system when using different mixing ratios for Products B and D respectively with silica sand under a constant mechanical loading. Before the wheel specimen comes into contact with the particles, the entire HPT system is in open circuit with infinite electrical resistance. Due to the mechanical action of the wheel specimen, the particles are gradually crushed, increasing their contact area with both the wheel and rail specimens. During this process, the fragments are detached from particles and realigned by the mechanical behaviour, and the conductive micro-channels for current transfer from wheel to rail specimen are built. At $t = 0.005$ s, the electrical resistance of the HPT system decreases to a measurable value. At the initial stage of the torsion of the rail specimen, the HPT resistance appears to fluctuate before stabilising. For 100 % silica sand particles, the high electrical resistivity of the sand particles prevents efficient current transmission through the fragment layer, leading to a resistance of 58 kΩ in the HPT system. However, the resistance of the HPT system drops dramatically when the proportion of conductive particles (Product B or D) in the test material increases to 5 %. As the percentage of conductive particles continues to increase to 30 %, the HPT system resistance decreases below 10 Ω, an acceptable resistance for these systems according to Skipper et al. [7].

Fig. 15 compares the effect of the size of conductive particle (i.e., using either Product B or D particles) at each mixing ratio on the HPT resistance in the final stage of the simulation. Although an effective reduction in the electrical resistance of the HPT system can be achieved by mixing either Product B or Product D particles in the silica sand particles, Product B reduces the electrical resistance of the HPT system better than Product D at the mixing ratios. This is because the particle size of Product B is smaller than Product D, so that for the same volumetric mixing ratio, more Product B particles are included, and thus more conductive micro-channels are built, as shown in Fig. 13a and b.

3.5. Effect of electrical resistivity of conductive particles on HPT resistance

The electrical resistivity of the investigated conductive particles Product D ranges from 4.31×10^{-5} to 1.66×10^{-8} Ω·m according to Skipper et al. [16]. To investigate how electrical resistivity of conductive particles effects the electrical resistance at the wheel-rail interface of the HPT system, the resistivity of Product D is altered, taking the resistivity value in Table 2 as a benchmark. The electrical resistivities of Product D particles used in the HPT model are listed in Table 4.

Fig. 16 shows that the electrical resistance of the HPT system is strongly influenced by both the proportion of Product D particles and its electrical resistivity. When the resistivity of Product D is constant, the electrical resistance of the HPT system decreases as the proportion of conductive particles increases, likely due to an increase in the conductive micro-channels in the fragment layer formed by contact paths, which are the main reason for current transfer under dry contact conditions [37]. When the proportion of conductive particles is constant, Fig. 16 shows a dramatic drop in the electrical resistance of the HPT system as the resistivity of Product D decreases from 10^{-5} Ω·m to 10^{-8} Ω·m. This occurs because lower resistivity more effectively reduces electron-atom collisions within the material, lowering electrical resistance and enabling more efficient current transfer through the conductive micro-channels in the fragment layer [38].

The above investigations have demonstrated that incorporating even a small amount of conductive material with low electrical resistivity into silica sand can significantly reduce the electrical resistance at the wheel-rail interface of the HPT system. Effective electrical conduction between the wheel and rail specimens is typically achieved when HPT electrical resistance falls below 10 Ω [7]. Both the resistivity of the conductive material and its proportion in the mixture play a critical role in determining the resistance of the HPT system. To better understand the relationship between electrical resistivity and the mixing ratio of conductive material, a contour cloud plot was generated using data from 25 simulations (Fig. 16). Interpolation was applied to enhance visualisation of the electrical resistance distribution under different conditions. Fig. 17 shows that selecting the appropriate resistivity and proportion of conductive material can reduce the HPT resistance below a critical threshold (10 Ω). Specifically, if the resistivity of the conductive material is less than 1×10^{-7} Ω·m, silica sand mixed with only 5 % of the conductive material to achieve good electrical contact. Conversely, if the resistivity of the conductive material is higher, a larger proportion of the material is required—potentially up to 100 % in some cases with high electrical resistivity values—to ensure effective electrical conduction in the HPT system.

4. Discussion

Building on experimental and numerical studies, this work summarises four distinct current transfer mechanisms at the wheel-rail interface, as illustrated in Fig. 18: (a) no particles, (b) the presence of only non-conductive particles, (c) a mixture of conductive and non-conductive particles, and (d) the presence of only conductive particles. Fig. 18a shows that in the absence of particles, at the microscopic level,

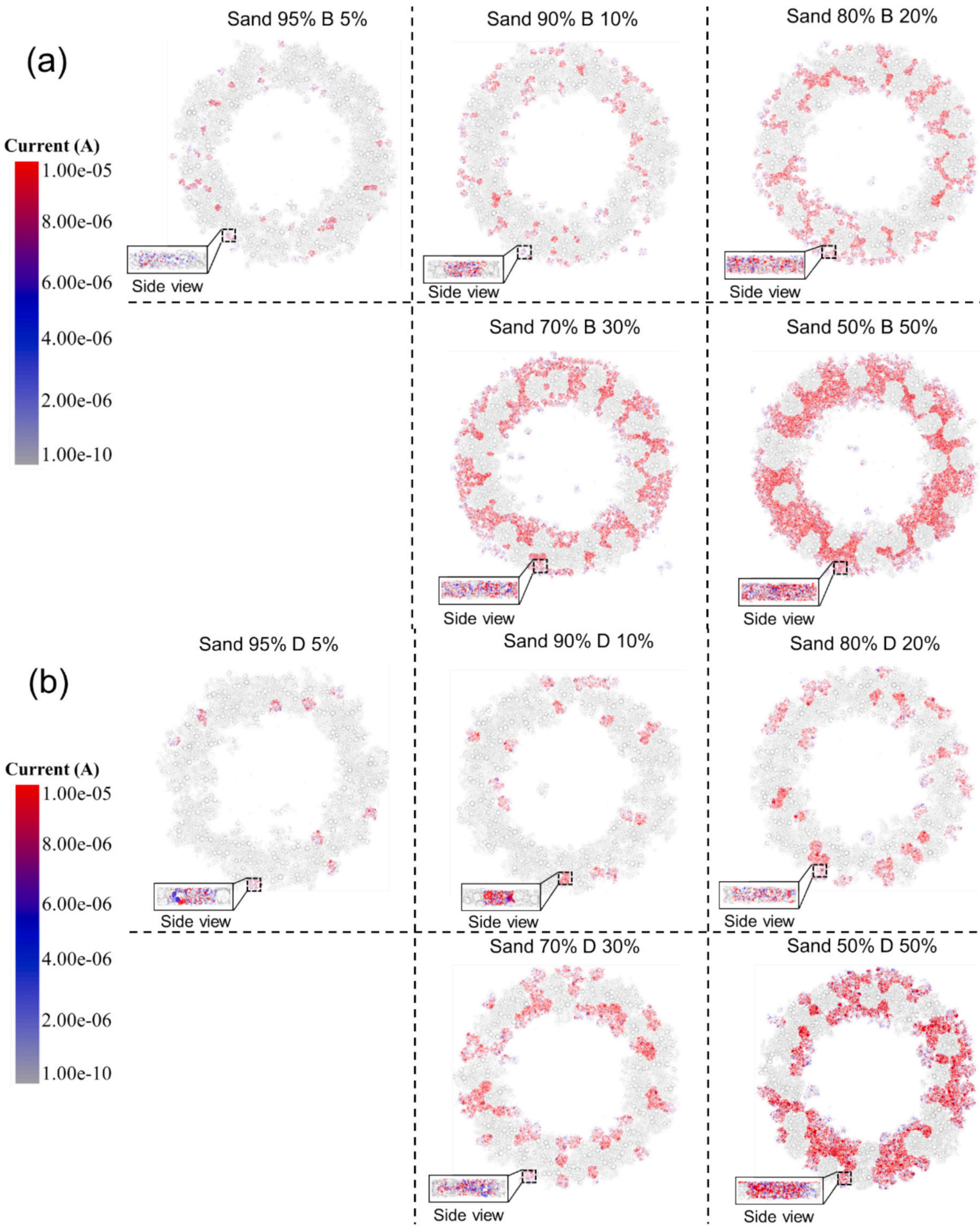

Fig. 13. Snapshots of the current intensity distribution in the fragment layer at the end of the simulation for silica sand mixed with (a) Product B and (b) Product D.

current flows through the asperities—tiny contact points—where the two metallic surfaces physically meet [39–42]. The mechanical forces increase the real contact area by deforming the asperities and breaking through any thin insulating layers that may form on the surface, such as oxides or contaminants. Fig. 18b illustrates current transfer when only non-conductive particles (e.g., silica sand) are present at the wheel-rail interface. The crushed particles form a dense, insulating fragment layer that prevents direct metal-to-metal contact, significantly restricting electron flow. As depicted in Fig. 18c, when a mixture of conductive and non-conductive particles is applied to the wheel-rail contact area, the mechanical loading leads to particle fragmentation and compaction, forming a dense fragment layer at the wheel-rail interface, commonly referred to as a friction film.[2] Although this fragment layer induces an indirect contact between the wheel and rail, the conductive fragments become distributed throughout the layer. Under continued mechanical loading, the contact area between these conductive fragments

[2] "Friction film" refers to a compacted layer formed at the interface due to particle fragmentation and compression under mechanical loading, which alters tribological and electrical properties.

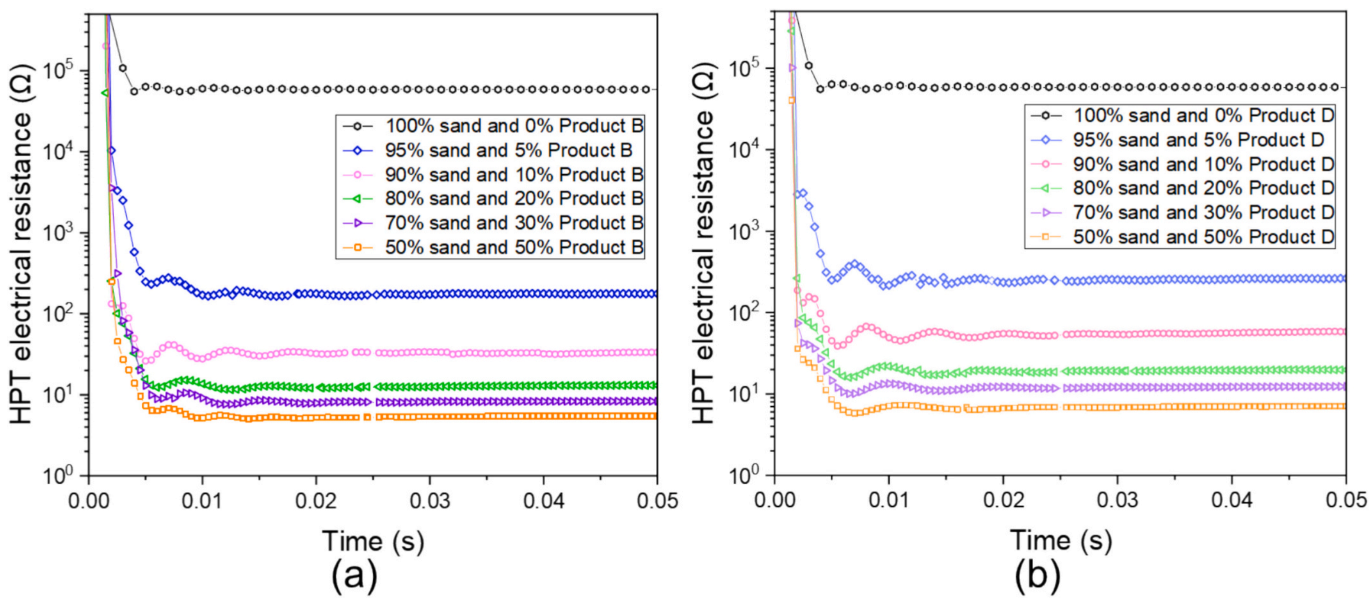

Fig. 14. The electrical resistance of the HPT system for each mixing scenario of conductive and non-conductive particles at constant mechanical load: (a) mixing of silica sand and Product B, (b) mixing of silica sand and Product D.

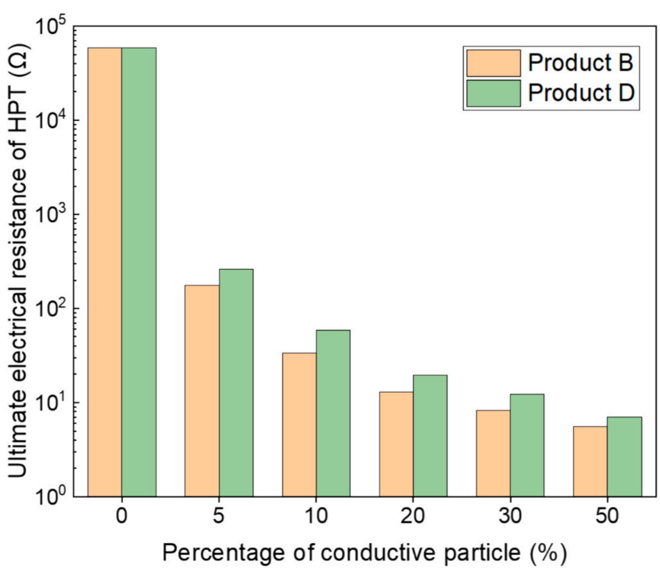

Fig. 15. Comparison of the effect of Products B and D on the ultimate electrical resistance of the HPT system at each mixing scenario.

Table 4
Resistivity values of Product D and sand particles used in the HPT simulation.

Case No.	Unit	Product D	Silica sand
1		4.31×10^{-5}	
2		5×10^{-6}	
3	Ω·m	1×10^{-6}	5.56×10^{6}
4		1×10^{-7}	
5		1.66×10^{-8}	

progressively increases, facilitating the formation of conductive microchannels. These channels enable the transfer of electrons from the wheel to the rail, thereby allowing partial electrical conductivity through the otherwise insulating friction film, and thus significantly reducing the electrical contact resistance at the interface. When all the

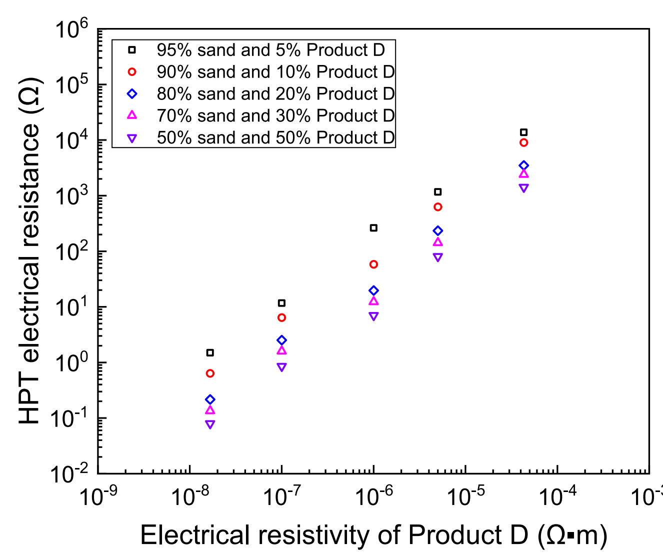

Fig. 16. Comparison of the effect of Product D with different resistivities on the electrical resistance of the HPT system.

particles present at the wheel-rail interface are conductive, their fragmentation results in the formation of a fragment layer that not only contributes to the repair of surface defects and interfacial microcracks on the wheel and rail but also facilitates electron transfer. In this scenario, the conductive fragment layer enables continuous and efficient electron flow from the wheel to the rail, ensuring effective electrical conductivity across the entire interface, as shown in Fig. 18d.

5. Conclusions and outlook

The present work proposes an approach for using a mixture of conductive and non-conductive particles at the wheel-rail interface. Combining laboratory tests and numerical simulations, the effect of mixing conductive and non-conductive particles in different ratios under mechanical loading on the electrical properties of the wheel-rail interface is analysed. The effect of the resistivity of the conductive particles

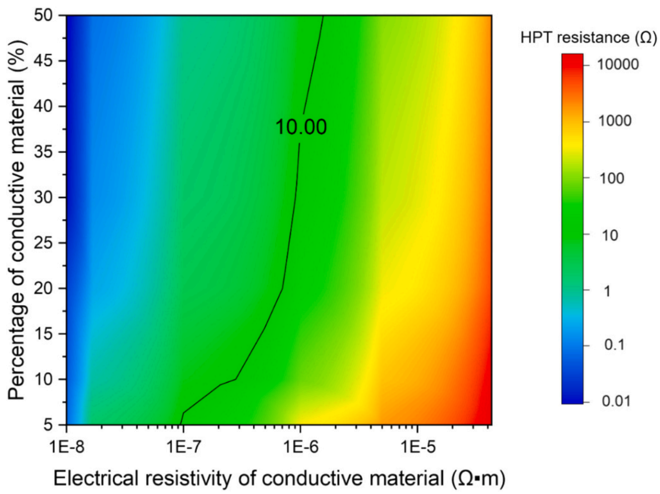

Fig. 17. Heatmap of electrical resistivity of conductive material versus its percentage for the electrical resistance estimation of the HPT system (Black line indicates the threshold value of 10 Ω [7]).

on the interfacial resistance is also investigated. The main findings are:

1) As the percentage of Product D particles increases, the electrical resistance at the interface of the piston and the base specimens decreases rapidly with the increasing load. In addition, when the load is maintained at 577 kN, the resistance at the interface decreases as the ratio of Product D in the mixture increases. In particular, the interfacial resistance drops sharply from about 55 kΩ to less than 220 Ω when the percentage of Product D increases beyond 5 %.
2) For Product D particles, their fragments are interspersed in the fragment layer during compression and conductive micro-channels are established. As the ratio of Product D increases, the tendency for localised charge build-up caused by the SiO_2 in the sand particles is gradually reduced, leading to improved conductivity in the fragment layer.
3) An increase in the proportion of either Product D or (the finer grained) Product B particles in the mixture can effectively minimise the resistance of the HPT system. When an equal content of Product B or D is mixed with sand particles, the finer fragments of crushed Product B particles with their larger surface area can better interpenetrate with the fragment layer, creating more conductive micro-channels. Therefore, the size of the conductive particles appears to be an important factor in reducing electrical resistance at the wheel-rail interface in HPT systems.
4) The electrical resistivity of the conductive material and its proportion in the mixture both strongly influence the electrical resistance at the wheel-rail interface of the HPT system. If a low-resistivity conductive material is mixed with silica sand, only a small percentage of conductive particles is needed to reduce the electrical resistance of the HPT system to less than 10 Ω. Conversely, if the resistivity of the conductive material is higher, a significantly larger proportion of the mixture must be conductive particles to achieve the same reduction in electrical resistance.
5) Future studies will investigate the effect of mixtures of conductive and non-conductive particles on the coefficient of traction (CoT) at the wheel-rail interface. The long-term environmental impact of introducing conductive particles into railway operations require further work. Lastly, given the potential segregation of conductive and non-conductive particles when mixed in sandboxes, future tests will examine how storage, vibration, and transport conditions affect their performance.

CRediT authorship contribution statement

Chao Zhang: Writing – review & editing, Writing – original draft, Software, Methodology, Investigation, Formal analysis. **Sadaf Maramizonouz:** Writing – review & editing, Supervision. **Changrong Yang:** Writing – review & editing, Methodology. **David Milledge:** Writing –

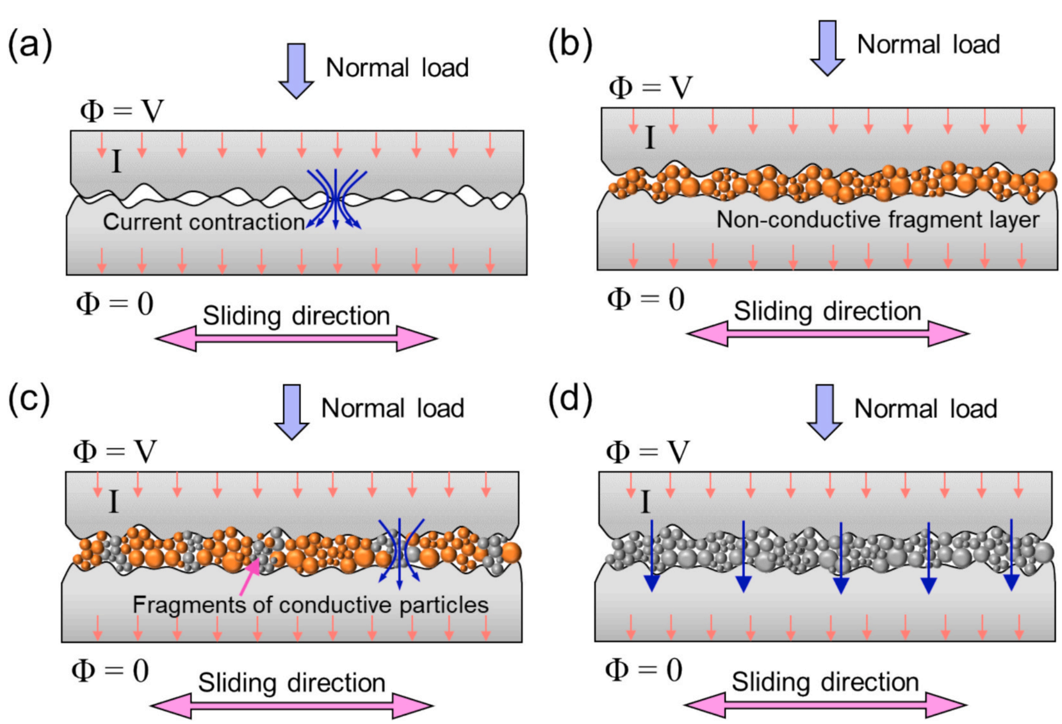

Fig. 18. Schematic of the effect of the particulate systems on the current transfer mechanism at the wheel-rail interface: (a) no particles, (b) non-conductive particles after crushing, (c) a mixture of conductive and non-conductive particles after crushing, and (d) conductive particles after crushing (Orange and grey spheres represent fragments for non-conductive and conductive particles, respectively).

review & editing, Supervision. **Roger Lewis:** Writing – review & editing, Supervision. **Sadegh Nadimi:** Writing – review & editing, Supervision, Resources, Conceptualization.

Declaration of competing interest

The authors declare that they have no known competing financial interests or personal relationships that could have appeared to influence the work reported in this paper.

Acknowledgements

The authors would like to extend their gratitude to Mr. Stuart Patterson and Mr. Gareth Wear of the Geotechnical Laboratory at Newcastle University for their kind assistance with the experiments. The authors would also like to express their sincere thanks to Dr. Isabel Arce-Garcia of the Electron Microscopy and Analysis Unit at Newcastle University for her kind assistance with the operation of the Scanning Electron Microscope (SEM).

Data availability

Data will be made available on request.

References

[1] W. Skipper, A. Chalisey, R. Lewis, A review of railway sanding system research: wheel/rail isolation, damage, and particle application, P I Mech Eng F-J Rai 234 (2020) 567–583, https://doi.org/10.1177/0954409719851634.
[2] Rail Accident Investigation Branch, Rail Accident Report: Near Miss between a Passenger Train and Cars at Norwich Road Level Crossing, New Rackheath, Norfolk (report 15/2020) [Online]. Available: https://www.gov.uk/raib-reports/report-15-slash-2020-near-miss-between-a-passenger-train-and-cars-at-norwich-road-level-crossing, 24 November 2019 (accessed August 11, 2024).
[3] Rail Safety and Standards Board, Optimising the ability of industry to deal with low wheel-rail adhesion and the use of sanders on train (T1046) [Online]. Available: https://www.rssb.co.uk/research-catalogue/CatalogueItem/T1046, 2015 (accessed August 5, 2024).
[4] W.A. Skipper, A. Chalisey, R. Lewis, A review of railway sanding system research: adhesion restoration and leaf layer removal, Tribol. - Mater. Surf. Interfaces 12 (2018) 237–251, https://doi.org/10.1080/17515831.2018.1542791.
[5] S. Nadimi, V. Angelidakis, M. Otsubo, A. Ghanbarzadeh, How can the effect of particle surface roughness on the contact area be predicted? Comput. Geotech. 150 (2022) 104890 https://doi.org/10.1016/j.compgeo.2022.104890.
[6] D. Krengel, H. Jiang, J. Chen, T. Matsushima, The combined effect of particle angularity and inter-particle friction on micro- and macroscopic properties of granular assemblies, Comput. Geotech. 177 (2025) 106850, https://doi.org/10.1016/j.compgeo.2024.106850.
[7] W. Skipper, S. Nadimi, D.V. Gutsulyak, J.G. Butterfield, T. Ball, R. Lewis, Investigating the effect of different adhesion materials on electrical resistance using a high pressure torsion rig, Wear 532–533 (2023) 205116, https://doi.org/10.1016/j.wear.2023.205116.
[8] Rail Safety and Standards Board, GMRT2461 Sanding Equipment (Issue 3) [Online], Available: https://www.rssb.co.uk/standards-catalogue/CatalogueItem/GMRT2461-Iss-3 (accessed June 26, 2022).
[9] T.M. Beagley, I.J. McEwen, C. Pritchard, Wheel/rail adhesion—boundary lubrication by oily fluids, Wear 31 (1975) 77–88, https://doi.org/10.1016/0043-1648(75)90123-4.
[10] T.M. Beagley, C. Pritchard, Wheel/rail adhesion — the overriding influence of water, Wear 35 (1975) 299–313, https://doi.org/10.1016/0043-1648(75)90078-2.
[11] L.E. Buckley-Johnstone, G. Trummer, P. Voltr, A. Meierhofer, K. Six, D.I. Fletcher, R. Lewis, Assessing the impact of small amounts of water and iron oxides on adhesion in the wheel/rail interface using high pressure torsion testing, Tribol. Int. 135 (2019) 55–64, https://doi.org/10.1016/j.triboint.2019.02.024.
[12] O. Arias-Cuevas, Z. Li, R. Lewis, Investigating the lubricity and electrical insulation caused by sanding in dry wheel–rail contacts, Tribol. Lett. 37 (2010) 623–635, https://doi.org/10.1007/s11249-009-9560-1.
[13] R. Lewis, R.S. Dwyer-Joyce, J. Lewis, Disc machine study of contact isolation during railway track sanding, Proc. Inst. Mechan. Eng. Part F J. Rail Rapid Transit. 217 (2003) 11–24, https://doi.org/10.1243/095440903762727311.
[14] E. Chapteuil, M. Renouf, C. Zeng, Y. Berthier, Influence of copper/graphite properties on the Tribological and electrical behavior of copper-graphite third body layer, Lubricants 6 (2018) 109, https://doi.org/10.3390/lubricants6040109.
[15] C. Zhang, S. Maramizonouz, D. Milledge, S. Nadimi, An electro-mechanical contact model for particulate systems, Powder Technol. 440 (2024) 119759, https://doi.org/10.1016/j.powtec.2024.119759.
[16] W. Skipper, S. Nadimi, R. Lewis, Sand Consist Change for Improved Track Circuit Performance (COF-UOS-03) 84, 2021.
[17] B. Suhr, W.A. Skipper, R. Lewis, K. Six, DEM simulation of single sand grain crushing in sanded wheel–rail contacts, Powder Technol. 432 (2024) 119150, https://doi.org/10.1016/j.powtec.2023.119150.
[18] S. Maramizonouz, S. Nadimi, W. Skipper, R. Lewis, CFD–DEM modelling of particle entrainment in wheel–rail interface: a parametric study on particle characteristics, Railw. Eng. Sci. (2025), https://doi.org/10.1007/s40534-024-00365-1.
[19] W.A. Skipper, S. Nadimi, M. Watson, A. Chalisey, R. Lewis, Quantifying the effect of particle characteristics on wheel/rail adhesion & damage through high pressure torsion testing, Tribol. Int. 179 (2023) 108190, https://doi.org/10.1016/j.triboint.2022.108190.
[20] L. Zhou, H. Brunskill, M. Pletz, W. Daves, S. Scheriau, R. Lewis, Real-time measurement of dynamic wheel-rail contacts using ultrasonic reflectometry, J. Tribol. 141 (2019), https://doi.org/10.1115/1.4043281.
[21] S. Maramizonouz, S. Nadimi, W. Skipper, R. Lewis, Characterisation of physical and mechanical properties of seven particulate materials proposed as traction enhancers, Sci. Data 10 (2023) 400, https://doi.org/10.1038/s41597-023-02304-x.
[22] British Standards Institution, BS 1377–2:1990 Methods of Test for Soils for Civil Engineering Purposes. Part 2: Classification Tests, British Standard, 1990.
[23] K. Bourbatache, M. Guessasma, E. Bellenger, V. Bourny, A. Tekaya, Discrete modelling of electrical transfer in multi-contact systems, Granul. Matter 14 (2012) 1–10, https://doi.org/10.1007/s10035-011-0307-y.
[24] M. Creyssels, C. Laroche, E. Falcon, B. Castaing, Pressure dependence of the electrical transport in granular materials, Eur. Phys. J. E: Soft Matter Biol. Phys. 40 (2017) 56, https://doi.org/10.1140/epje/i2017-11543-3.
[25] P.A. Cundall, O.D.L. Strack, A discrete numerical model for granular assemblies, Géotechnique 29 (1979) 47–65, https://doi.org/10.1680/geot.1979.29.1.47.
[26] C. Thornton, Granular Dynamics, Contact Mechanics and Particle System Simulations, Springer International Publishing, Cham, 2015, https://doi.org/10.1007/978-3-319-18711-2.
[27] A. Mikrajuddin, F.G. Shi, H.K. Kim, K. Okuyama, Size-dependent electrical constriction resistance for contacts of arbitrary size: from Sharvin to Holm limits, Mater. Sci. Semicond. Process. 2 (1999) 321–327, https://doi.org/10.1016/S1369-8001(99)00036-0.
[28] O. Wing, Circuit Theory with Computer Methods, Holt, Rinehart and Winston, New York, 1972.
[29] C.-W. Ho, A. Ruehli, P. Brennan, The modified nodal approach to network analysis, IEEE Trans. Circuits Syst. 22 (1975) 504–509, https://doi.org/10.1109/TCS.1975.1084079.
[30] R. Holm, The contact resistance. General theory, in: R. Holm (Ed.), Electric Contacts: Theory and Application, Springer, Berlin, Heidelberg, 1967, pp. 9–11, https://doi.org/10.1007/978-3-662-06688-1_3.
[31] H. Hertz, Ueber die Berührung fester elastischer Körper 1882, 1882, pp. 156–171, https://doi.org/10.1515/crll.1882.92.156.
[32] Altair EDEM. https://2021.help.altair.com/2021.1/EDEM/index.htm, 2021.
[33] W. Skipper, R. Lewis, D. Fletcher, Understanding how railhead and wheelset contamination affects track circuit performance: evaluation of datasets (T1222) [Online], 2023. Available, https://www.sparkrail.org/Lists/Records/DispForm.aspx?ID=27732.
[34] Y. Wang, P. Mora, Y. Liang, Calibration of discrete element modeling: scaling laws and dimensionless analysis, Particuology 62 (2022) 55–62, https://doi.org/10.1016/j.partic.2021.03.020.
[35] D.O. Potyondy, P.A. Cundall, A bonded-particle model for rock, Int. J. Rock Mech. Min. Sci. 41 (2004) 1329–1364, https://doi.org/10.1016/j.ijrmms.2004.09.011.
[36] C. Zhang, S. Nadimi, S. Maramizonouz, D. Milledge, R. Lewis, A discrete element model of high-pressure torsion test to assess the effect of particle characteristics in the interface, J. Tribol. 146 (2024) 081501, https://doi.org/10.1115/1.4065230.
[37] Y.-L. Yang, T. Zhang, S.-Y. Liu, Influence factor analysis and calculation model for thermal/electrical resistivity of geomaterials, Measurement 152 (2020) 107373, https://doi.org/10.1016/j.measurement.2019.107373.
[38] C.E. Housecroft, A.G. Sharpe, Structures and energetics of metallic and ionic solids, Inorg. Chem. 2008 (2008) 164–171.
[39] B. Brodnik Zugelj, M. Kalin, Submicron-scale experimental analyses of the multi-asperity contact behaviour of various steels, an aluminium alloy and a polymer, Tribol. Int. 141 (2020) 105955, https://doi.org/10.1016/j.triboint.2019.105955.
[40] X. Liu, M. Hu, Z. Li, C. Zhou, Q. Xiao, W. Yang, D. Chen, Effect of copper contents on the current-carrying wear properties of carbon brush under different temperatures conditions, J. Mater. Res. Technol. 15 (2021) 3110–3121, https://doi.org/10.1016/j.jmrt.2021.09.111.
[41] B.N.J. Persson, On the electric contact resistance, Tribol. Lett. 70 (2022) 88, https://doi.org/10.1007/s11249-022-01630-2.
[42] C. Zhai, D. Hanaor, G. Proust, L. Brassart, Y. Gan, Interfacial electro-mechanical behaviour at rough surfaces, Extreme Mech. Lett. 9 (2016) 422–429, https://doi.org/10.1016/j.eml.2016.03.021.